Journal of Fluids and Structures 70 (2017) 374–389

Contents lists available at ScienceDirect

Journal of Fluids and Structures

journal homepage: www.elsevier.com/locate/jfs

Current blockage in sheared flow: Experiments and numerical modelling of regular waves and strongly sheared current through a space-frame structure

H. Santo[a,*,1], D. Stagonas[b], E. Buldakov[b], P.H. Taylor[a]

[a] Department of Engineering Science, University of Oxford, Parks Road, Oxford OX1 3PJ, United Kingdom
[b] Department of Civil, Environmental and Geomatic Engineering, University College of London, Gower Street, London WC1E 6BT, United Kingdom

ARTICLE INFO

Keywords:
Current blockage
Porous block
Sheared flow
Morison drag loading
Actuator disc

ABSTRACT

Space-frame structures supporting marine renewable energy machines such as offshore wind turbines are exposed to complex hydrodynamic forces resulting from the coexistence of waves and currents. Previous investigations on the interaction of such a structure acting as an obstacle array with regular waves and in-line uniform current reported a reduced fluid loading due to current blockage. This paper documents laboratory-scale experimental evidence for reduced fluid loading on a truss structure exposed to regular waves with in-line sheared current in shallow water. Strongly sheared current of different speeds is generated and profiled using purposely-built wire resistance arrays in a wave-current flume, and a range of regular waves are created using a piston-type wavemaker. The global hydrodynamic force time history on a truss structure is measured for a range of sheared current speeds and regular wave heights. For all test cases, two loading configurations are considered, with the truss positioned end-on and diagonal to the incident flow direction. Comparisons are made with the analytical current blockage model for steady uniform current by Taylor (1991) and Taylor et al. (2013), and with the numerical simulations conducted in OpenFOAM using a porous tower model following the approach by Santo et al. (2015a). Under the same input condition, the diagonal loading configuration is observed to attract higher forces and therefore the orientation of the structure plays an important role when assessing the survivability of such structures. Overall, good agreement in terms of the peak forces and the shapes of force time histories is achieved for all cases with an inline current, all with a single and consistent value for each of the local Morison drag and inertia coefficients (here $C_d \sim 2.1$ and $C_m \sim 2$), with the coefficients defined in terms of the overall structure. In contrast, predictions using the present API recommendation with the same C_d and C_m result in force overpredictions for all cases of regular waves with in-line current. For steady sheared current flow through a porous tower, apart from the dominant lateral flow divergence, numerical flow visualisation reveals the existence of vertical flow interaction in the porous tower. This is attributed to the non-uniform loading with water depth and was not observed previously for uniform current flow. This study provides the first experimental validation and justification for the use of a simple porous block in representing a complex geometry of real space-frame structures when exposed to combined large regular waves and in-line current.

* Corresponding author.
E-mail address: ceehs@nus.edu.sg (H. Santo).
[1] Present address: Centre for Offshore Research & Engineering, Department of Civil and Environmental Engineering, National University of Singapore, 1 Engineering Drive 2, Singapore 117576, Singapore.

http://dx.doi.org/10.1016/j.jfluidstructs.2017.02.010
Received 19 September 2016; Received in revised form 19 December 2016; Accepted 14 February 2017

1. Introduction

An early study of current blockage without accounting for the presence of waves was reported by Taylor (1991) using 1D actuator disc theory, which was subsequently incorporated into the API design guidelines in 1994 (American Petroleum Institute, 2000) as part of the standard design recipe for space-frame offshore structures. Recent work by Taylor et al. (2013) demonstrated analytically additional blockage to be gained by accounting for the presence of regular waves with an in-line current, which improves the Morison equation (Morison et al., 1950). This has been validated extensively through experimental tests and numerical modelling using porous blocks by Santo et al. (2014a,b, 2015a). An extension of the current blockage model to account for wave irregularity with the presence of current is presently on-going, and will be reported elsewhere. All the aforementioned work considers uniform flow with and without regular waves present.

The current blockage model by Taylor (1991) was developed for spatially uniform current. Recently, for the application of marine/current turbines in shallow water, Draper et al. (2016) developed a model to assess turbine performance in inviscid shear flow using 2D actuator line theory. This work could be potentially applied to current blockage problem in sheared flow, and further extended to blockage in regular waves with an in-line sheared current, although this aspect is not explored in this paper.

This work extends the current blockage problem to strongly sheared current flow, which is a more realistic representation of a current flow in some regions in the open sea, see e.g. Chakrabarti (1996), Lueck and Lu (1997), Forristall and Cooper (1997), Sanford and Lien (1999), Stacey et al. (1999). The presence of sheared currents has been reported in flow field measurements at locations of particular interest to the marine renewable energy sector, such as the Pentland Firth separating the Orkney Islands from the north coast of Scotland. Examples of strongly sheared tidal current profiles from the EMEC tidal energy test site at the Fall of Warness in the Orkney Islands are shown by Gunn and Stock-Williams (2013). Their Fig. 11(a) shows a remarkable range of profile shapes in 35 m of water, all with a depth-averaged current of 1–1.2 m/s. Some profiles have the largest velocity at the free-surface, a few close to the bed and some in mid-column, and all strongly dependent on the state of the tide (flood or ebb, accelerating or decelerating). Thus, the fluid flow of the sheared current profile in such location occupies a significant portion of the water column with non-negligible velocities (Stagonas et al., 2016). Hence, it differs from a typical wind-driven type of sheared current generated in most of previous experimental studies of regular waves on currents, where the velocity rapidly reduces from a maximum at the free-surface to nearly zero at a relatively small distance underneath. Here, simple close to linearly sheared currents are experimentally generated with and without regular waves and the fluid force exerted on a truss model is measured. The experimental apparatus and the numerical wave tank are described in Sections 2 and 3. Results are presented and discussed in Section 4, and the paper is concluded in Section 5.

2. Experimental setup

The experiments were conducted at a 20 m long×1.2 m wide×1 m deep wave-current flume in University College London (UCL), with the schematic diagram shown in Fig. 1. This 'up-welling' type facility has the water recirculated by a system of pumps and the flow is vertically introduced (inlet) and removed (outlet) through 0.4 m deep settling tanks located at 1 m in front of two wavemakers positioned at each end of the flume. These Edinburgh Design Limited (EDL) 'piston-type' wavemakers are equipped with force-feedback and operated such that when waves are generated by either one of them the other moves to absorb the incoming wave energy. The flow is treated to the desired sheared profile using an in-house designed, built and tested, conditioning and profiling system, see Figs. 1 and 2. The system was extensively tested by Stagonas et al. (2016), and it was shown to be efficient for the creation of relatively stable sheared currents of different speeds and the combined generation of waves on these currents. Nonetheless, the interaction of the propagating waves with the vertically discharged flow and the conditioner/profiler sets a physical limit to the steepest waves that could be produced without wave breaking at a short distance from the wavemaker. A similar experimental setup was also used to assess loads on surface-piercing cylinders with focussed wave groups with and without a similar sheared current profile, see Stagonas et al., (2014, 2015).

A space-frame (or truss) structure representing a support frame for an offshore wind turbine, or at slightly larger field scale an offshore oil platform, was mounted on a rigid frame placed on top of the flume, and was positioned at 8.8 m away from the wavemaker assigned for generating waves. The truss model is made of aluminium, with a cross-section of 0.117 m×0.117 m, and with the length extending almost to the bottom of the flume with 5 mm clearance. Four vertical cylinders with a diameter of 2.5 cm form the legs of the model, and these are connected with diagonal bracings with a diameter of 0.65 cm. Four additional vertical tubes of 0.65 cm diameter were added on each vertical side of the structure to increase the relative importance of drag over inertia forces. The top plate arrangement connecting the truss model and the support frame was designed in such a way to allow both end-on (0°

Fig. 1. Schematic side view of the UCL wave-current flume (not to scale) showing two wavemakers at each end of the flume, locations of inlet and outlet of the current discharge, the flow conditioner and the profiler.

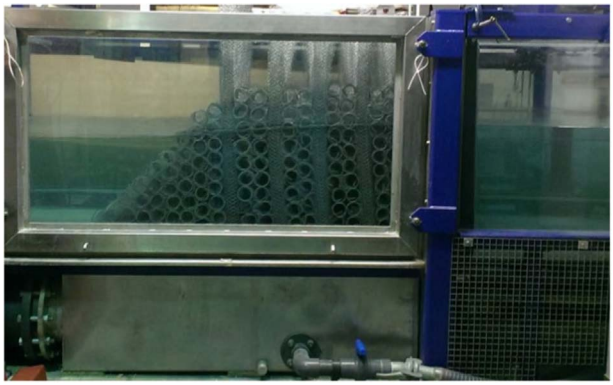

Fig. 2. Photograph of the conditioning and profiling system positioned at the inlet of the flume.

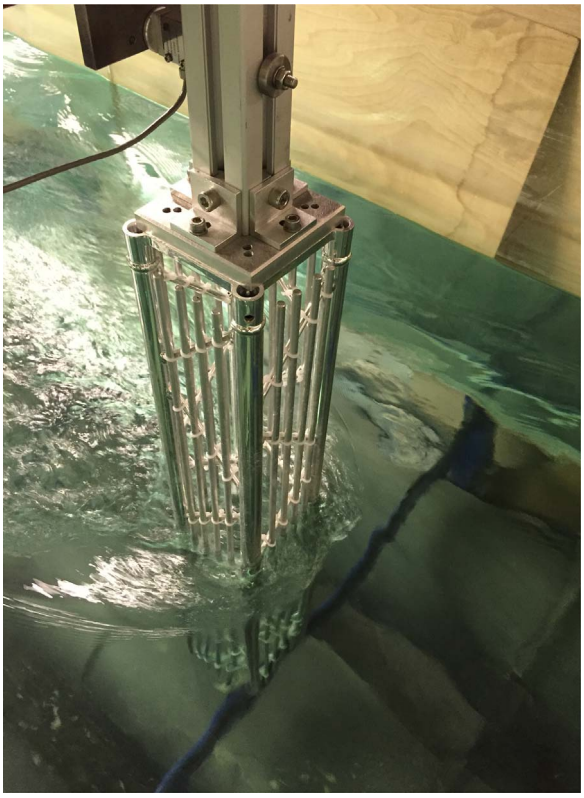

Fig. 3. Photograph of the truss model (end-on configuration) showing the top plate arrangement and one of the load cells. The truss was subjected to steady sheared current flow, with the resultant global flow divergence around the structure and the wake structure downstream.

incident loading) and diagonal (45° incident loading) configurations without the need to remove the whole support structure. Fig. 3 shows a photograph of the truss model and the wake in a mean flow. A detailed schematic drawing of the truss, together with the loading orientation, is provided in Fig. 14 in the Appendix.

For all experiments reported here, the water depth was set at 0.5 m. Two strongly sheared current velocities were used, each with a maximum velocity at free-surface of 0.2 and 0.4 m/s, respectively, as the base cases for combination with regular waves. The current profiles are shown in Fig. 4. Regular waves of varying wave height at the wavemaker were generated, ranging from 0.035 m up to 0.075 m, all at 1 Hz frequency in order to reproduce the intermediate depth conditions anticipated in most areas where such space-frame structures might be deployed. The upper range of regular wave height corresponds to the highest wave conditions achievable experimentally without triggering wave breaking near the conditioner/profiler, hence the generated waves in this

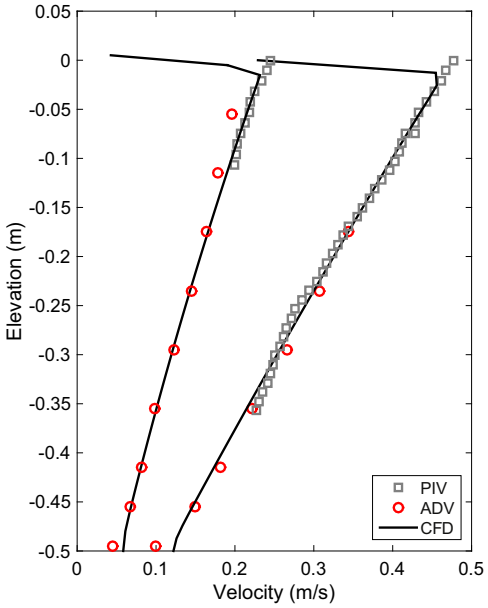

Fig. 4. Comparison of the sheared current profile with depth in terms of measurements (ADV and PIV) and numerical simulations at the location of the model for two different current velocities, i.e. u_c=0.2 (left) and 0.4 m/s (right).

experiment were not that steep, representing an operational condition for a wind turbine support structure rather than a survival condition. This limitation does not apply to the numerical simulations, where steeper waves can be achieved. For a typical velocity of 0.2 m/s and a vertical cylinder diameter of 2.5 cm, the Reynolds number is ~1300.

Two load cells, rated at 25 kg (245 N), were used to extract the global horizontal force by solving a simple system of a static beam with two supports. The load cells were positioned at dry locations, 0.65 m and 0.8 m above still water level and were sampled at 1 kHz. In order to achieve accurate force measurements, a calibration procedure was applied to forces ranging from 0 to 8.16 kg (80 N), see Fig. 15 in the Appendix.

For regular waves with and without current, the surface elevation was measured using a resistance type wave probe, sampled at 100 Hz, and positioned at the side of the model structure at a distance of 0.25 m from the sidewall and 8.8 m from the wavemaker. At this location, the characteristics of the wave interacting with the structure are well described without being contaminated by unwanted effects occurring near the wavemaker and the inlet of the physical wave-current flume. Measurements of the surface elevation next to the model provide the phase information required for decomposing the measured total force into a sum of drag and inertia forces, and it is also helpful for comparison with numerical simulations. For all tests, both surface elevation and total force were simultaneously measured. The total force measurement was subsequently low-pass filtered with cutoff at 6 × the input wave frequency, the force results presented here are virtually unchanged for cut-offs at >4 × the wave frequency. The filtered total force was decomposed into combination of drag and inertia force following the decomposition method successfully applied in Santo et al. (2014b).

In addition to force and surface elevation time histories, undisturbed flow kinematics (without the presence of the truss model) were also measured for sheared current only using combination of acoustic doppler velocimetry (ADV) and particle image velocimetry (PIV). The flow kinematics at the structure location were measured with a Vectrino+ ADV by Nortek-AS equipped with a side looking probe and set at its maximum sampling frequency of 25 Hz, while the measurement volume was set at 9.2 mm and the acoustic pulse length at 2.4 mm. The flow was seeded with rutile titanium dioxide pigment and only data with correlation values higher than 85% were considered for the calculation of the mean velocity in 3 min long records collected at each of the 9 measuring locations through the water depth. For regions closer to the free-surface where the intrusive nature of the instrument results in deterioration of the quality of the measured signal, the ADV results were complemented with PIV measurements acquired at 250 fps, see Fig. 4. The laser of the PIV system was introduced from the bed of the flume shining upwards, and the camera was set at the side of the flume, both at a distance of 8.8 m from the wavemaker. The PIV system was also used to measure flow kinematics in focused waves on sheared currents and the details will be reported in a follow-up work.

3. Numerical setup

The numerical setup is similar to that reported by Santo et al. (2015a), using the same porous block/tower approach in OpenFOAM® (http://www.openfoam.com) and the numerical wave tank 'waves2Foam' developed by Jacobsen et al. (2012). Similar work have been conducted on characterising resistance based on drag and Morison equations in related fields, see e.g. Zhao et al. (2013), Kristiansen and Faltinsen (2012) and Chen and Christensen (2016).

3.1. Governing equations

The governing equations for the two-phase combined flow of water and air are the Reynolds-averaged Navier–Stokes equations coupled with the continuity equation for incompressible flows, with an additional momentum sink term to account for the effect of the porous tower in the numerical simulation:

$$\nabla\cdot\mathbf{u} = 0 \tag{1}$$

$$\frac{\partial\rho\mathbf{u}}{\partial t} + \nabla\cdot[\rho\mathbf{u}\mathbf{u}^T] = -\nabla p^* + \nabla\cdot[\mu\nabla\mathbf{u} + \rho\boldsymbol{\tau}] - \mathbf{S} + [-(\mathbf{g}\cdot\mathbf{x})\nabla\rho + \sigma_T\kappa_\gamma\nabla\gamma] \tag{2}$$

where ρ is the fluid density, $\mathbf{g}$ is the acceleration due to gravity, $\mathbf{u} = (u, v, w)$ is the fluid velocity field in Cartesian coordinates, p^* is the pressure in excess of hydrostatic pressure, defined as $p^* = p - (\mathbf{g}\cdot\mathbf{x})\rho$, μ is the dynamic viscosity, $\mathbf{x} = (x, y, z)$ is the local Cartesian coordinates, and $\boldsymbol{\tau}$ is the specific Reynolds stress tensor. All the simulations are performed in two-phase flow by solving the Navier-Stokes equations, and the free surface (interface between air and water) is tracked using Volume-of-Fluid (VOF) method, see Berberović et al. (2009) for more details of the interface treatment.

A sink term is used to account for momentum lost from the flow, which in the case of a simple homogeneous porous tower can be written as:

$$\mathbf{S} = \frac{1}{2}\rho F\mathbf{u}|\mathbf{u}| + C'_m\frac{\partial\rho\mathbf{u}}{\partial t} \tag{3}$$

where F is the Forchheimer resistance parameter and C'_m is the equivalent of the standard Morison inertia coefficient, C_m, but here defined in the porous tower context. Following Santo et al. (2014a), (2015a), the following relationship holds for the calibration of the Forchheimer resistance (F) parameter: $C_dA/A_f = FL$, where A is the solid drag area, A_f is the frontal area of the truss structure, and L is the downstream length of the porous tower. Because the truss structure is made of predominantly vertical cylinders, and assuming C_d is constant for both end-on and diagonal loading, the product of C_dA is constant for both loading configurations. Therefore, F for diagonal loading will be different from F for end-on loading because L and A_f will be different. Hence, for both end-on and diagonal loading, we calibrate the F parameters directly from the sheared current flow measurements using numerical simulations. C_d can then be inferred using the above relationship. The local Morison inertia coefficient for porous tower, C'_m, is modelled by equating $C'_m = C_mV/V_P$, where V is the displaced volume of the elements in the truss structure, and V_P is the volume of the porous tower.

As raised by one of the reviewers, our formulation of momentum and continuity accounting for porous tower flow is indeed different to the implementation as described in Jensen et al. (2014) which is applied to flow modelling over coastal porous structures. It is worth remarking that here we completely remove the effect of finite volume of solid, and replace the solid bluff body by a distributed stress over the enclosed volume. The reduced velocity that is being numerically solved represents the mean velocity over the projected frontal area of the structure modified by bulk effect of the structure as obstacles (current blockage). In other words, in our flow modelling over a porous tower, there is no account for the physical volume of the structural elements within the numerical cells (no 'pore velocity representation'), nor there is for local velocity amplification due to the presence of other members, i.e. the flow being accelerated as it goes through the holes/gaps. Hence, our calibrated values of C_d and C_m are slightly higher compared to those appropriate for the same structural members in isolation.

3.2. Boundary and initial conditions

The sheared current profile was generated in the numerical wave tank by specifying the steady horizontal velocity profile, which varies with water depth, at both the inlet and outlet to ensure mass conservation in the tank. This numerical approximation inevitably induces some artificial internal circulation, hence the zone of interest including the location of the porous tower had to be placed nearer to the inlet and at sufficiently far distance away from the outlet to ensure the flow solutions were not affected by the approximation. The horizontal velocity profile was obtained by curve fitting the measured (experimental) horizontal velocity profile at the model location using a quadratic polynomial expression. We performed runs for two different sheared current profiles, and obtained stable propagation of the sheared current along the numerical wave tank in both space and time. Slip boundary conditions are applied along the side walls and the floor of the numerical wave tank. All other initial and boundary conditions followed the same set-up as described in Santo et al. (2015a).

It is worth remarking that our method of generating sheared current is different to that of Fleming et al. (2013) who applied

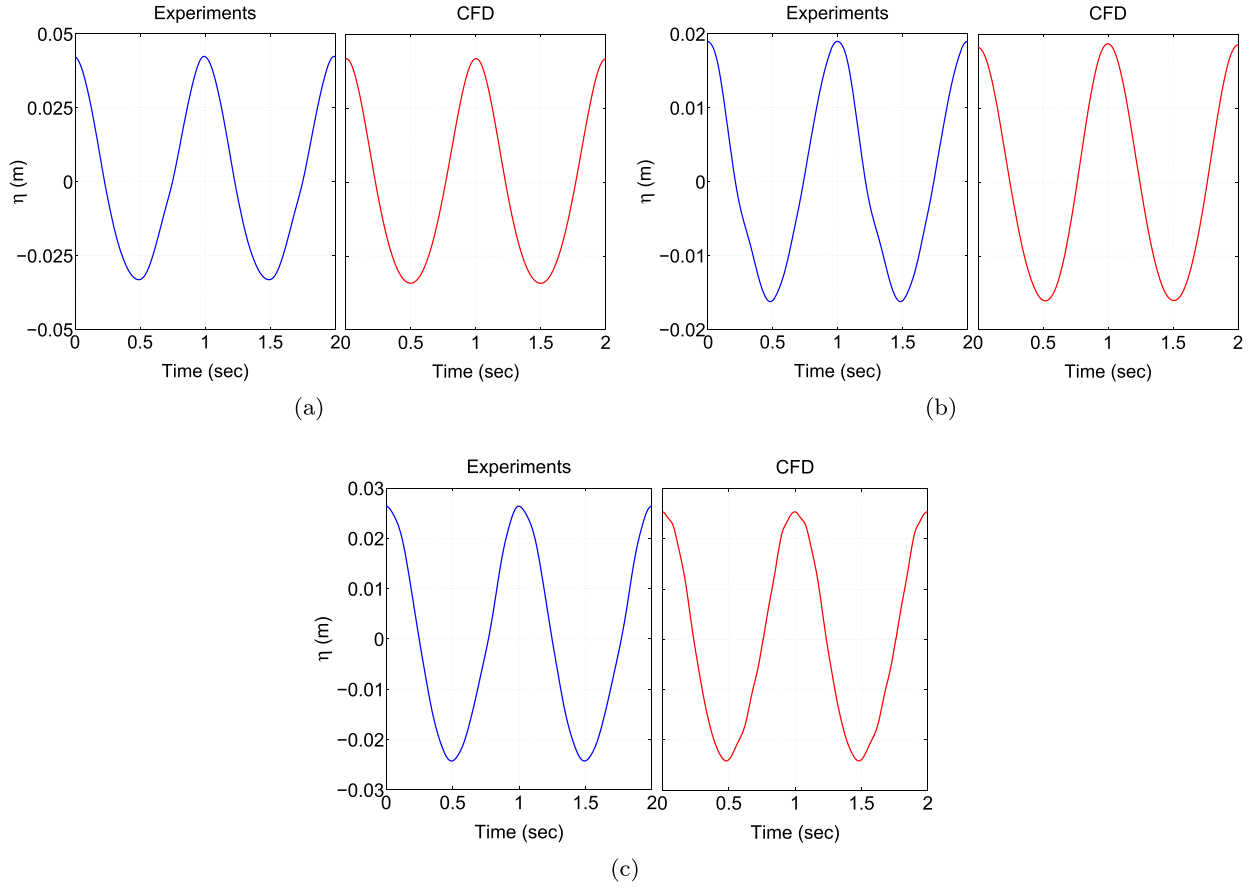

Fig. 5. Comparison of surface elevation time history next to the model between experiments (left) and numerical simulations (right) for the case of (a) regular waves of height ~0.077 m, (b) regular waves of height ~0.035 m and in-line sheared current of 0.2 m/s, and (c) regular waves of height ~0.05 m and in-line sheared current of 0.4 m/s.

shear stress on the bottom boundary to generate the desired sheared flow profile for flow approaching a marine current/tidal turbine, with associated turbulent intensity, kinetic energy and dissipation rate. Because of our method of generating sheared profiles using the upstream input, no turbulence was generated inside the fluid domain other than turbulent shear layers shed through the edges of the porous tower, or turbulence injected from the inlet. Arguably this is adequate for our application in fluid loading over a space-frame structure. The turbulence generated as shear layers along the edges of the porous tower helps to mix the resultant wake and the outer undisturbed flow before the ambient flow is partially recovered at some distance downstream of the tower, see Santo et al. (2014a). Here we use an LES (Large Eddy Simulation) k-equation eddy-viscosity to model the turbulent mixing, consistent with our previous work in Santo et al. (2015a). We stress that although LES is used in this paper, comparable results can be obtained by any turbulence models including RANS models. We have also run cases with a RANS $k-\omega$ turbulence model and obtain virtually identical results. This is because of the use of a porous tower to represent the truss model, where the flow can still partially flow through the body having a prescribed resistance. Hence, there are no violent flow perturbations, strong flow separation nor boundary layers generated in the simulations, unlike the case with a single resolved bluff body with no slip boundary conditions. Therefore, our results using LES can be equivalently regarded as a RANS solution.

Fig. 4 presents the comparison of sheared current profile with depth in terms of measurements (combination of ADV and PIV) and numerical simulations (CFD) at the location of the model for two different current cases. A stable sheared current profile both in time and space can be obtained in the numerical simulations, and good agreement with the measured profiles is achieved. Some discrepancy can be observed near the free surface where the effect of finite mesh size defining the interface between air and water is important.

Stokes 2nd order wave theory was imposed at the inlet to generate regular waves in the tank. For combined waves and current, the exact experimental condition was reproduced in the numerical wave tank by superimposing the regular wave and sheared current at the inlet. Fig. 5 shows the comparison of surface elevation time histories between experiments and numerical simulations for cases of regular waves without and with sheared current, which has been averaged cycle-by-cycle over several wave periods. The

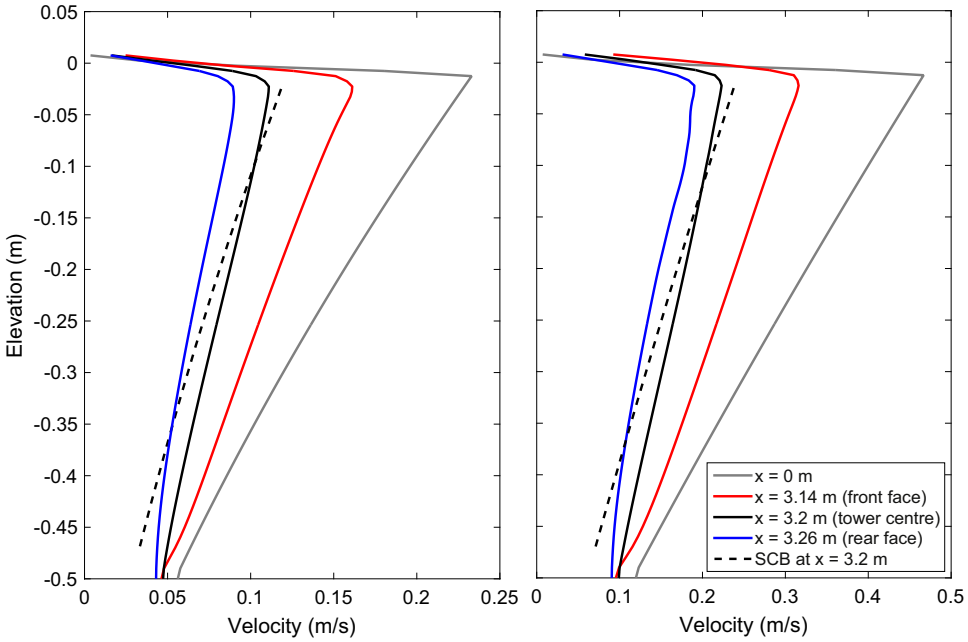

Fig. 6. Evolution of the numerical sheared current profile with depth (solid lines) at several locations from the inlet and the comparison with the simple current blockage predictions (dashed lines) at the tower centre for two different current velocities, i.e. u_c=0.2 (left) and 0.4 m/s (right).

surface elevation was measured out to the side of the model structure towards the side wall of the tank. In general, good agreement with the measured time histories is achieved.

In our simulations, the sheared profile was initialised throughout the computational domain. The simulation was run until the current and wave-current interaction with the porous tower reached steady-state (or simple periodic for waves and current) behaviour, by examining the total force time history on the tower. For the case of regular waves with in-line sheared current, at least 8–10 wave periods was required. All computations were run in parallel mode on 16 processors at the High Performance Computing facilities of the University of Oxford.

Just as the empirical drag and inertia coefficients (C_d and C_m) are required for the prediction of wave forces on the structure using the standard Morison equation, it is necessary to specify the resistance parameter in our porous tower simulation. For both loading configurations, we obtain an estimate of bare 'unblocked' C_d=2.12. Note that for this low Reynolds number flow, our numerical estimate of C_d compares reasonably well with the C_d from the numerical simulation of closely spaced cylinder arrays of Kevlahan and Ghidaglia (2001). In all cases, we assume C_m=2.0, which is the potential flow-based value for vertical cylinders.

It is worth stressing that in the actual physical experiments, the resistance is effectively restricted to the surface of the enclosed volume. However, our calibration of F and C'_m parameters assumes that the density of the drag (area) and inertia (volume) of the actual truss structure are uniformly distributed over the depth of the structure in the same manner as the porous tower, which turns out to be a satisfactory assumption in this case.

4. Results and discussions

In this section, the numerical results for both end-on and diagonal loading are presented for a range of sheared current velocities and regular wave heights. We consider a 3D computational domain spanning from 0 m (inlet) to 12 m (outlet) in streamwise direction, with the porous tower located at 3.2 m from the inlet. The width of the domain is 1.2 m, and the height is 1 m, with the water depth set at 0.5 m from the bottom. The porous tower is made of a square cross-section of 0.12 m by 0.12 m, and the height is 0.7 m (protruding above the water surface). Hence, L=0.12 m and A_f=0.06 m^2. In the numerical simulations, the x coordinate runs horizontally in the direction of wave propagation, the y coordinate runs horizontally in the orthogonal direction of wave propagation (or laterally) and the z coordinate runs vertically (+ve upwards). The numerical prediction of the forces is obtained by depth integration of the disturbed flow kinematics in the wetted portion of the porous tower in a similar manner as described in Santo et al. (2015a).

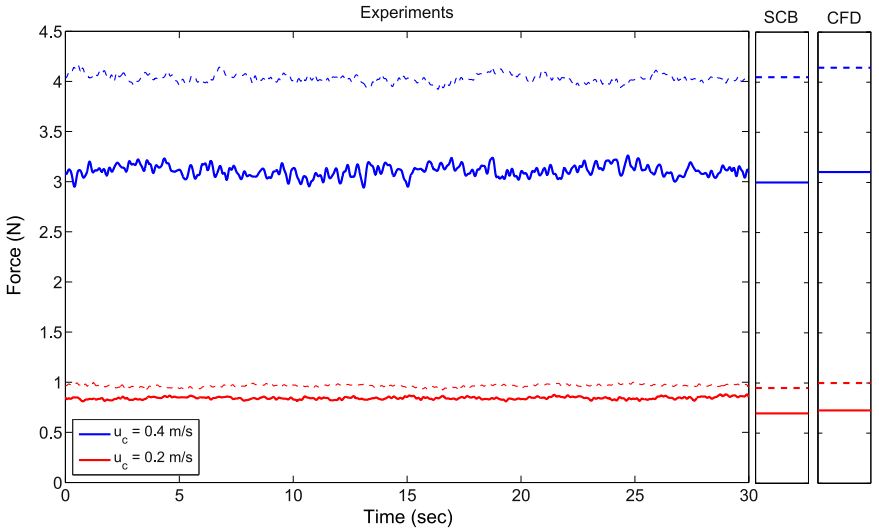

Fig. 7. Drag force comparison between experiments, analytical simple current blockage model (SCB) and numerical simulations (CFD) for four different current velocities and two different model configurations, i.e. end-on (solid lines) and diagonal (dashed lines).

4.1. Sheared current flow only

Here, a steady sheared current through a porous tower is simulated and the results are compared with experiments and predictions from the simple current blockage (SCB) model. Following Taylor (1991) and Taylor et al. (2013), the SCB model predicts that the blocked current, u_{cs}, can be expressed in terms of the free-stream current, u_c, as:

$$u_{cs} = u_c \Big/ \left(1 + \frac{C_d A}{4A_f}\right). \tag{4}$$

To obtain the force predictions from the SCB model, a stick model which comprises a series of vertically-stacked actuator discs is used to represent the truss structure, with each disc acting independently of each other (no vertical flow interaction between each adjacent disc). A can be taken as constant for the end-on and diagonal loading configuration since the truss model is made up of predominantly vertical cylinders. Hence, since everything else is constant other than A_f, according to the prediction from SCB, the diagonal loading configuration will have smaller blockage or force reduction compared to the end-on loading configuration under the same input condition.

Fig. 6 shows the evolution of the numerical sheared current profile with depth (solid lines) for u_c=0.2 (left) and 0.4 m/s (right) at several locations around the porous tower (one inside, the other two at front and rear faces), taken along y=0 which is along the centreline of the tower. The wake structure downstream of the tower is not shown but this will be visible from Fig. 8 on flow visualisation. As expected, flow reduction is observed when the incident sheared flow encounters the porous tower. Note that because of the lateral flow divergence inside the tower, the reduced flow profile varies along the lateral width (y) of the porous tower. It is of interest to explore if there is any vertical interaction/mixing apart from the usual lateral flow divergence (as seen in Fig. 3), as one might expect from a non-uniform loading on a porous tower with a uniform resistance distribution. As a preliminary assessment on the amount of vertical interaction/mixing that might occur in sheared flow, the prediction from the SCB model neglecting any vertical interaction is added on the same figure as dashed lines, and the comparison is made at the tower centre. Reasonably good agreement between the two predictions suggests there is relatively small vertical interaction inside the porous tower, and perhaps the interaction through lateral flow divergence is more dominant. The existence of such vertical flow interaction can also be observed directly from the variation of the flow reduction across the water depth, which is non-uniform; there is more flow reduction at the upper portion of the water column compared to the lower portion. This suggests there is some vertical flow interaction occurring around and inside the porous tower.

Fig. 7 summarises the comparison in terms of drag force between experiments and predictions from the SCB and the numerical simulations (CFD) for two different current velocities and two different loading configurations, i.e. end-on (solid lines) and diagonal (dashed lines) loading. For the SCB predictions, the measured frontal area, A_f, has to be increased by 10% to obtain a good match with the experiments for end-on loading, while for diagonal loading, the frontal area is taken to be $\sqrt{2}\times$ the frontal area of the end-on loading (0° incident loading), which is essentially the maximum projected frontal area for 45° incident loading, see Santo et al. (2014a) for steady flow analysis on skew grids. For the end-on configuration, if the C_d is chosen to fit the drag force for u_c=0.2 m/s

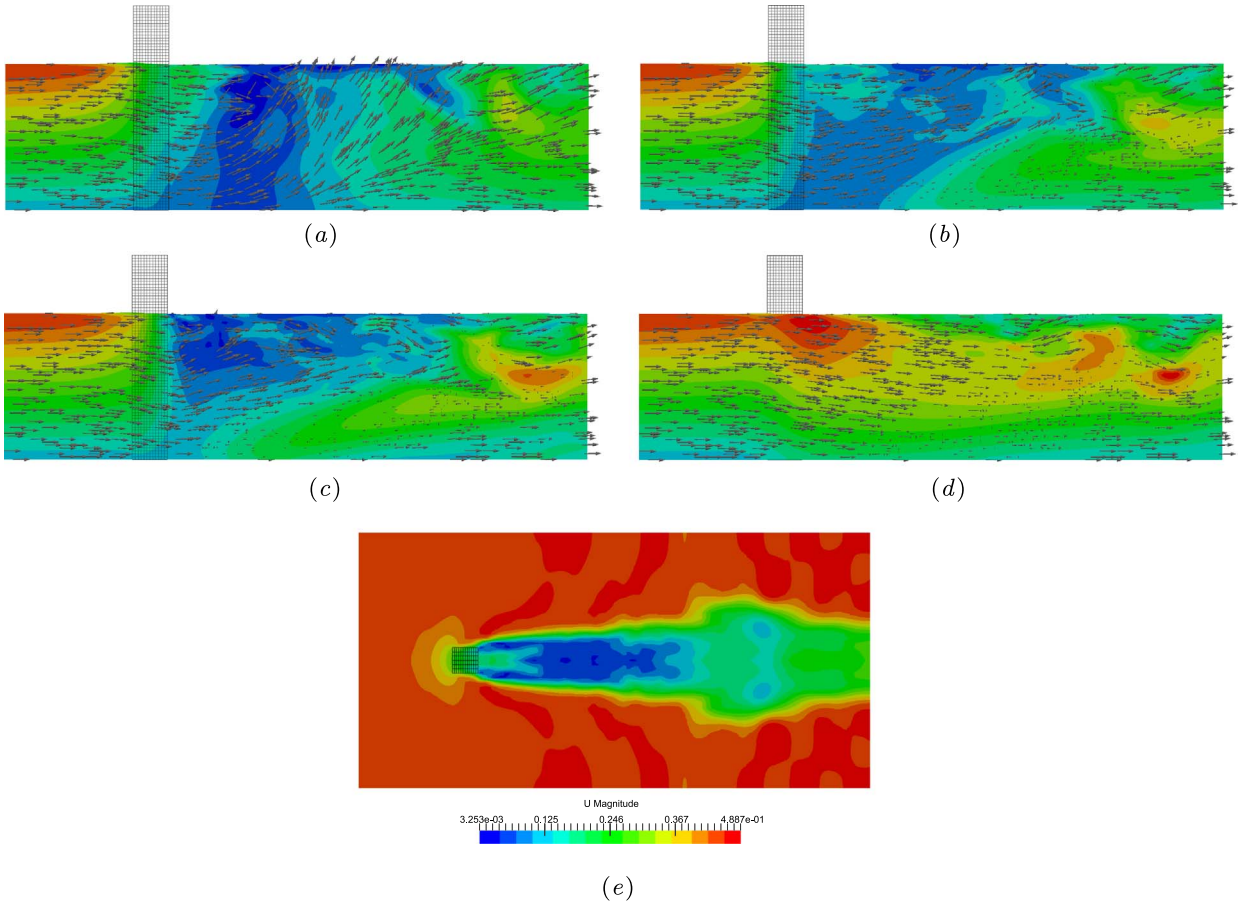

Fig. 8. Numerical flow visualisation of the flow taken within the central portion of the computational domain. The porous tower location is indicated by a block of black coloured mesh, while the flow is coloured based on the magnitude of the velocity. Subfigure (a)–(d) shows the flow visualisation taken from a vertical slice. The component of the flow velocity vector is shown as a grey arrow. Vertical slices of (a), (b), (c) and (d) refer to lateral distance of y=0 m, 0.03 m, 0.06 m and 0.12 m, respectively. Subfigure (e) shows the flow visualisation taken from a horizontal slice at $z = -0.1$ m, where z=0 corresponds to the mean water level.

case, the drag force predictions from both SCB and CFD will be overpredicted for u_c=0.4 m/s case. This is most likely due to in-line effects on the sides of the truss parallel to the flow, hence we are likely to be overestimating the drag on the small 0.65 cm vertical members on the sides which are directly in the wake of the larger front legs. From the figure, the diagonal loading configuration is observed to result in higher drag forces compared to the end-on configuration, and the difference in the drag forces increases as the current speed increases. Each individual case can be reproduced with satisfactory agreement using both analytical and numerical modelling with C_d=2.12 for all cases. The reasonable agreement between the experiments and SCB model further justifies the observation that most of the flow interaction inside the truss structure occurs laterally rather than vertically, and the use of SCB model which is essentially a series of actuator disc stacked on top of each other is appropriate in that manner. We will return to this discussion shortly afterwards.

The fact that the SCB predictions are always smaller than the numerical predictions could be partly due to 'wind-tunnel blockage' – the effect of the geometric blockage ratio, defined as the ratio of frontal area of structure divided by cross sectional area of the flow, as pointed out by one of the referees. For the end-on loading configuration, the blockage ratio is 10%, which is not insignificant, and the ratio is higher for the diagonal configuration. Following Garrett and Cummins (2007), for example with a structure having $C_d A/A_f = 2.0$, a blockage ratio of 10% will increase the force by 10% compared with the same structure in an indefinitely wide cross section, and one should correct for this when fitting C_d using the analytical SCB model. This is perhaps also the reason why we needed to increase A_f by 10% for the analytical predictions to match the measurements better. However, since the fitting was also performed via numerical simulations, which include 'wind-tunnel' geometric blockage, and the focus of this paper is on the numerical modelling, we choose to retain C_d=2.12 for all cases.

A simple estimated uniform profile of the averaged mean flow as a substitute for the sheared profile can be obtained from the SCB model (or the API-type Morison calculation). For sheared profile with u_c=0.2 m/s and 0.4 m/s, the mean flow is found to be 0.15 m/

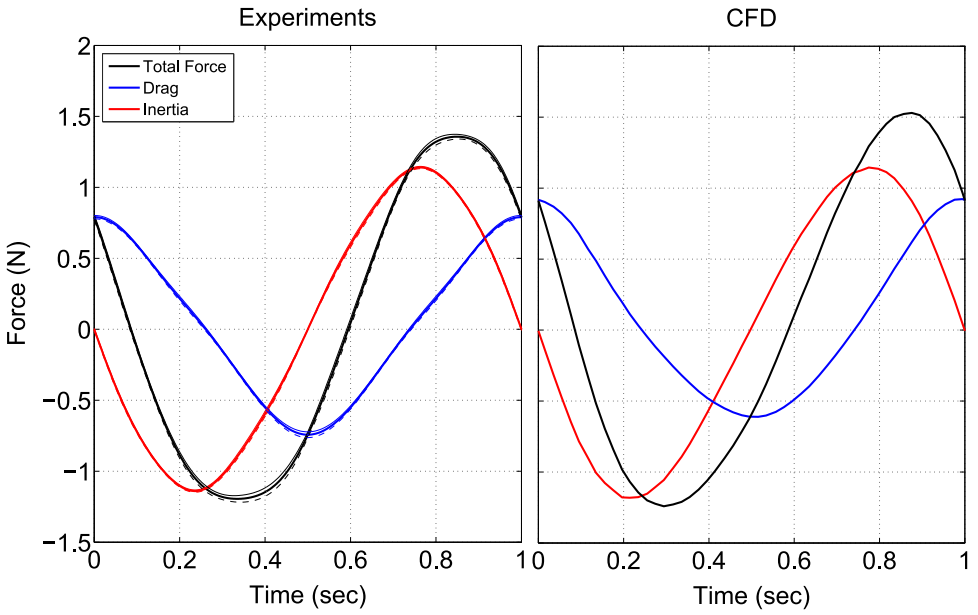

Fig. 9. Force time history comparison between experiments (left) and numerical simulations (right) for the case of regular waves of height ~0.06 m for the end-on loading configuration. Total force, drag and inertia components are plotted as solid black, blue and red lines, respectively. The thin solid and dashed lines for forces in experiments represent ± 1 standard deviation for the variation of the mean.

s and 0.31 m/s uniform across the water depth, respectively. This mean uniform current flow would produce the same overall drag force on the truss model as the sheared current profile, after accounting for the blockage effects.

Fig. 8 presents numerical flow visualisation of the behaviour of the sheared current in the presence of a porous tower, taken within the central portion of the computational domain. The location of the tower is indicated by a block of black coloured mesh, while the colour in the flow represents the magnitude of the velocity. Figs. 8(a)–(d) show vertical slices taken along different lateral width, y. The lateral dimension of the tower extends from $y = -0.06$ to y=0.06 m, centred at y=0 m, hence Figs. 8(a)–(c) show vertical slices within the width of the tower for three different lateral distances, while Fig. 8(d) shows a slice beyond the tower width. The component of the flow velocity vector in the visualisation plane is shown as a grey arrow on the figure. Because the flow visualisation is taken from a vertical slice, laterally diverging flow (with direction normal to the slice) is not shown. However, the existence of such diverging flow can be observed from Fig. 8(e) which shows the plan view or horizontal slice of the flow. All flow visualisation is taken when the flow reaches a steady-state condition. The air phase is not shown.

Fig. 8(a) illustrates the flow behaviour along the lateral centreline of the porous tower. Inside the tower, one can see the tendency of the flow to flow downward to the lower (deeper) portion of the water column (looking at the vector field), as well as the usual lateral diverging flow (normal to the slice) which is not visible in this vertical. This is expected because in sheared flow, the upper portion of the water column moves faster than the lower portion and this induces higher loading and hence higher resistance (blockage). This causes the tendency of the flow to go downwards. Immediately downstream of the tower, since the flow reduction is larger at the upper portion than the lower portion (hence the pressure is lower at the upper portion), one can see the tendency of the flow at the lower portion to flow back up to the upper portion. Subsequently, the reduced flow recovers partially to the ambient flow at sufficiently far downstream. A similar behaviour is illustrated in Fig. 8(b), even though the reduction is smaller than what would occur along the centreline, due to the contribution from the lateral diverging flow. Fig. 8(c) shows strong reduction at the upper portion of the water column immediately downstream of the tower, which is associated to shear layers shed through the edges of the porous tower. The observed flow behaviour downstream of the tower is similar in general. Fig. 8(d) shows the behaviour of the flow at a slice 0.12 m away from the tower centreline. The longitudinal flow velocity is seen to increase as a result of the lateral flow divergence away from the tower. Downstream of the tower, a weaker interaction between the ambient and the reduced flow at the upper half of the water column is observed. The resultant lateral flow divergence around and within the porous tower, as well as existence of shear layers shed through the edges of the tower, is best illustrated by looking at the horizontal slice as shown in Fig. 8(e). The wake structure is clearly visible downstream of the tower, which exhibits complex structure due to stronger vertical flow interaction. On the other hand, for uniform current flow through a porous tower as observed by Santo et al. (2015a), the resultant mean wake structure is relatively simpler, with the width of the global wake observed to be fairly constant before it slowly narrows far downstream. In summary, the observed vertical interaction (or mixing) in sheared current flow is significantly different to what was previously observed for uniform current flow through a porous tower, where there is very little vertical interaction.

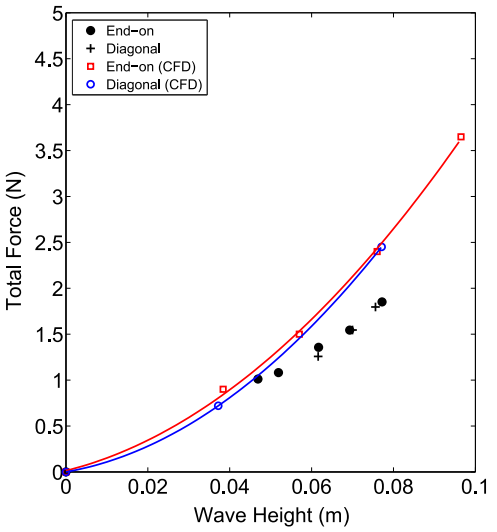

Fig. 10. Comparison of the measured (data points) and simulated (solid lines with data points) total forces for a range of regular waves only under both end-on and diagonal loading configurations.

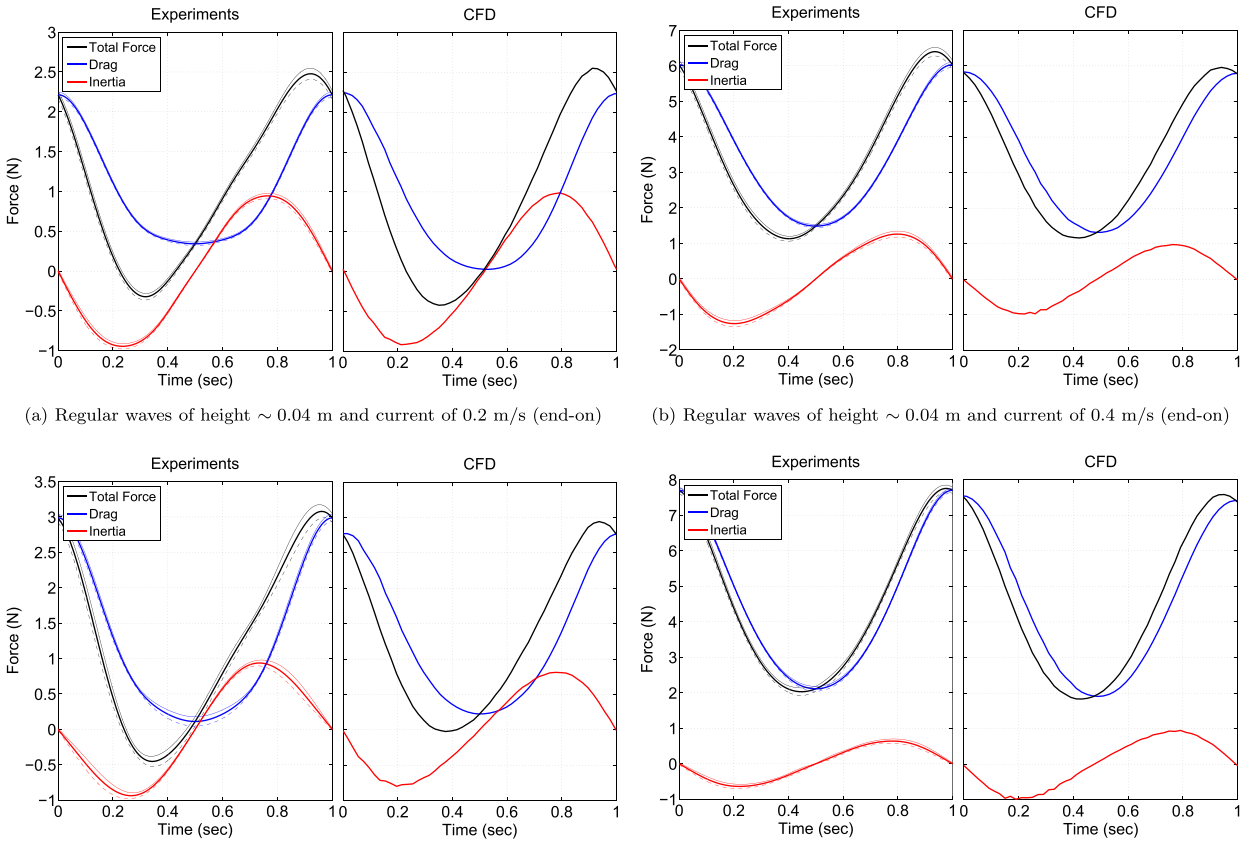

(a) Regular waves of height ∼ 0.04 m and current of 0.2 m/s (end-on)

(b) Regular waves of height ∼ 0.04 m and current of 0.4 m/s (end-on)

(c) Regular waves of height ∼ 0.042 m and current of 0.2 m/s (diagonal)

(d) Regular waves of height ∼ 0.042 m and current of 0.4 m/s (diagonal)

Fig. 11. Force time history comparison for each subfigure between experiments (left) and numerical simulations (right). Total force, drag and inertia components are plotted as solid black, blue and red lines, respectively. The thin solid and dashed lines for forces in experiments represent ± 1 standard deviation for the variation of the mean.

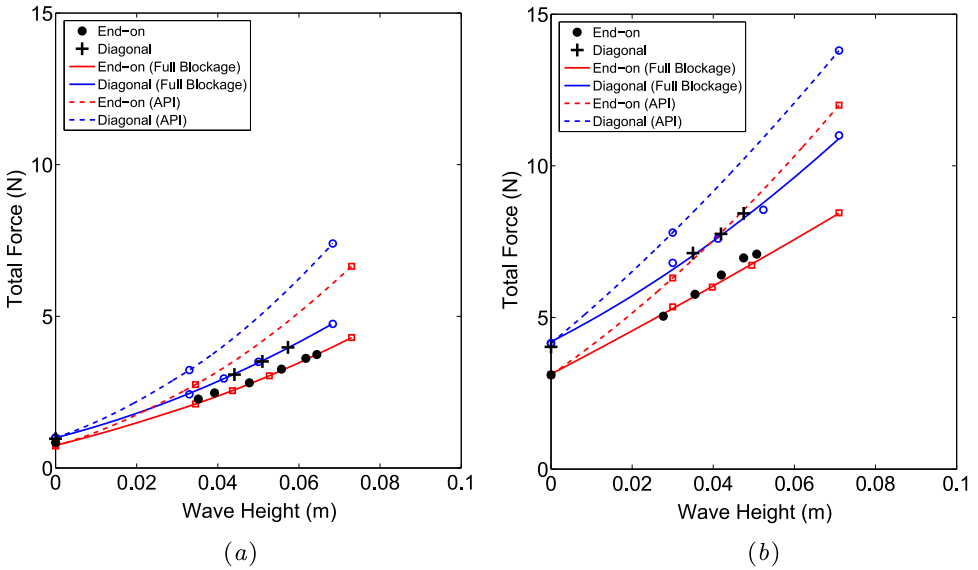

Fig. 12. Comparison of the measured (data points) and simulated (lines with data points) total forces for a range of regular waves and in-line sheared current of (a) 0.2 m/s and (b) 0.4 m/s, all for both end-on (red) and diagonal (blue) loading configurations. Solid colour lines show the numerical predictions accounting for full wave-current blockage effects, and dashed colour lines show the numerical predictions according to the present API recipe, all using the same C_d and C_m. (For interpretation of the references to color in this figure legend, the reader is referred to the web version of this article.)

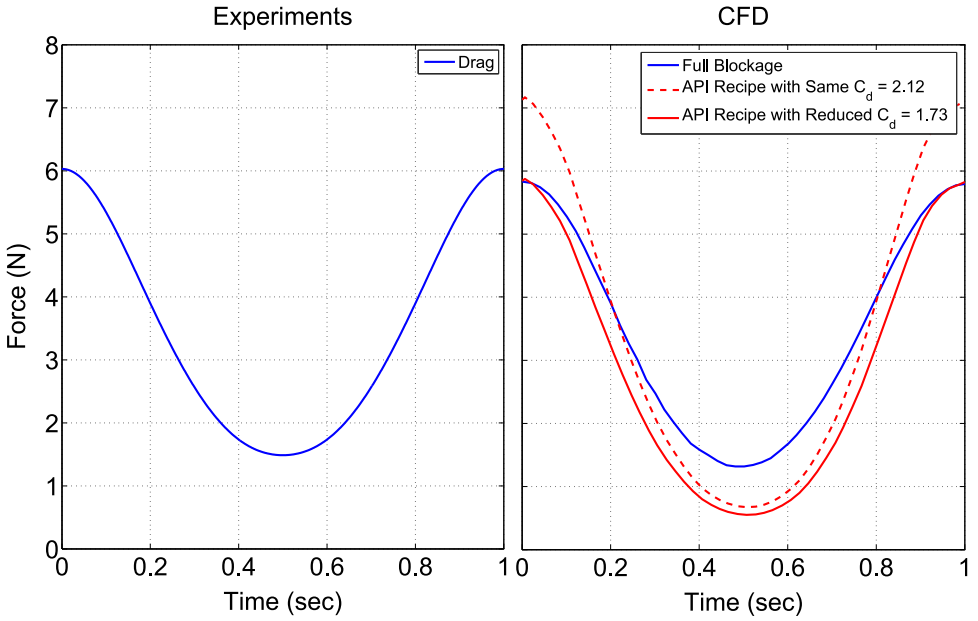

Fig. 13. Comparison of the measured (left) and simulated (right) drag force time histories for the case of regular waves of height ~0.04 m and in-line sheared current of 0.4 m/s for the end-on loading configuration.

4.2. Regular waves only

Having calibrated C_d from the experimental measurements of steady sheared current flow only, we proceed with numerical simulations of regular waves assuming C_m=2.0. Fig. 9 presents a comparison of force time history between experiment and numerical simulation for regular waves of height ~0.06 m with the truss model positioned end-on to the incident flow. Total force, drag and inertia components are plotted as solid black, blue and red lines, respectively, and the thin solid and dashed lines for forces in experiments represent ± 1 standard deviation for the variation of the mean. The measured total force is initially decomposed into drag and inertia forces, and each force component is then averaged (cycle-by-cycle) over 25 wave periods acquired during steady-state periodic conditions to minimise effects due to initial transients. The inertia force is reproduced well, but the drag force is

slightly overpredicted. In general for smaller wave height where the inertia force is observed to dominate over the drag force, the measured shape of the force time histories can be reproduced in reasonably good agreement with the numerical simulation.

Any wave blockage effect due to Stokes drift downstream is small and there is no build up of a global mean wake (hence no occurrence of current blockage), the standard Morison equation (Morison et al., 1950) might be expected to be adequate in describing the total force. Because the truss model was made of predominantly vertical tubes, the drag area is comparable for the end-on and diagonal loading configuration. Hence, the total force for both loading configurations is also comparable under the same input condition. Fig. 10 summarises the experimental results (data points) for all regular wave cases in terms of total peak force against wave height for both loading configurations. Also shown is the numerical predictions for both loading configurations (solid lines with data points), with data points represent the simulated cases and solid lines are the interpolated results. Reasonably good agreement is achieved between the measured total forces and the numerical predictions for smaller wave heights. As the wave height increases, the drag force becomes more important, hence the drag force and the resultant total force are consistently over-predicted using the same C_d and C_m. Effectively, C_d needs to be reduced for larger waves with no current, which is presumably a wake-related effect: being affected by wake re-encounter and the wave amplitude, and captured by the variation with Keulegan-Carpenter number. Of course the experiment are also at a rather low Reynolds number. However as will be demonstrated in the next subsection, as soon as a steady current is introduced, a constant set of values C_d=2.12 and C_m=2.0 works well for all cases.

4.3. Regular waves with an in-line sheared current flow

Having presented results for regular waves, we proceed with numerical simulations of regular waves with in-line sheared current using the same and consistent C_d and C_m coefficient values.

Fig. 11 presents force time history comparisons between experiments (left) and numerical simulations (right) for ~0.04 m regular waves with in-line sheared current of 0.2 and 0.4 m/s, respectively, both for end-on and diagonal loading. As the speed of the sheared current is increased, one can see the increased dominance of the drag over inertia force components. For similar incident wave heights but with increasing current speed, the inferred inertia force increases by ~25% and the temporal shape becomes more distorted (skewed) for the larger current. This is in contrast to the predictions from the numerical simulations which exhibit little change in the peak inertia force as the current is increased, consistent with the observation of rather small change in inertia forces in the previous simulations of regular waves with in-line uniform current by Santo et al. (2015a). We do recognise the possible role of the Froude-Krylov force in this context, with our previous experience suggesting that there is a partial contribution from the convective derivative to the total inertia load (Santo et al., 2015b). The simulated shape of the drag force in time is in reasonably good agreement with the measured drag, apart from a slight over-prediction of the trough of the drag force for the smaller current for end-on loading. Overall, the measured shape of the force time history as well as the peak values are reasonably well reproduced in the numerical simulations, all using the same and consistent C_d and C_m values. The good agreement provides support to the use of a Morison stress-distributed porous tower in the numerical modelling as a simple representation of a complex array of cylinders used in the experiments and/or real space-frame offshore structures.

Fig. 12 summarises peak values of the measured total forces (data points) for a range of regular waves with 0.2 and 0.4 m/s in-line sheared current for the end-on and diagonal loading configuration. Also shown is the numerical predictions (solid coloured lines with data points – full blockage) for each case, with data points represent the simulated cases and solid coloured lines the interpolated results. Now, good agreement is obtained between the measured results and the numerical predictions. It is obvious that because the diagonal loading has smaller blockage compared to the end-on loading, the resultant force is higher for the diagonal loading under the same input condition, and the difference increases as the current speed increases. This highlights the importance of considering the diagonal loading configuration when assessing the survivability of fixed space-frame offshore structures, especially since the diagonal case is a more critical arrangement in terms of foundation loads to be carried by the piles or other foundation system.

On the same figure, the predictions according to the present API recipe (or SCB) is shown as dashed coloured lines with data points. The predictions due to the present API recipe are obtained by running the same simulations without the presence of the tower, hence using undisturbed flow kinematics, but with reduced current profile according to the recipe (or SCB, see Eq. (4)). Similar behaviour between the predictions according to API and full blockage is observed: the diagonal case results in larger total force than the end-on case. Having calibrated C_d coefficient from steady sheared current case, applying the API recipe keeping the same C_d and C_m=2.0 for all cases will over-predict the measured total force when regular wave is present with the in-line current. This demonstrates the additional blockage due to waves that is not accounted for in the present API (or industry) recipe. It is worth emphasising that the height of regular waves considered here are of low to moderate steepness because of the physical constraint in the wave-current flume experiments. In the case of a storm where the wave induced horizontal velocities are much larger than the current speed (representing an extreme event), the difference in the peak forces between the present API recipe and the full blockage recipe becomes much larger.

Arguably one can tune the empirical coefficients, in particular the C_d values, to match the peak force using the present API recipe. However, one needs to use different C_d values for steady sheared current only, and for every case of regular waves with different heights with in-line current, consistent with the observations from Allender and Petrauskas (1987). Even with the tuned C_d values, the predicted complete shape of the (drag) force time history will be different to the measurement, as investigated experimentally in

detail in Santo et al. (2014b). Here, the difference in the overall shape of the drag force over a 3D truss structure is investigated. Fig. 13 presents an example for the same case of regular waves of height ~0.04 m and in-line sheared current of 0.4 m/s for the end-on loading configuration. The comparison is made in terms of drag force time history between the measurement, the full blockage, and the present API formulation. It is clear from the comparison that with the tuned (or reduced) C_d values, the crest of the drag force time histories from the API formulation can be matched to that of the measurement and the full blockage recipe, but nowhere else away from the crest. Hence, it is evident that there is more force reduction associated with the presence of regular waves with in-line current on top of the existing reduction due to steady current (as outlined in the present API recipe). This extra force reduction is captured reasonably well by the numerical model using a porous block with an embedded Morison resistance approach, both in terms of the peak forces as well as the complete force time histories using a single set of consistent C_d and C_m values.

Using flow visualisation in the numerical simulations, we compare the flow behaviour due to regular waves with in-line sheared current to that due to regular waves with in-line uniform current as described in Santo et al. (2015a). There is considerable similarity in the flow behaviour at the porous tower and downstream of the tower. Similar vortex 'breakdown' is observed at a distance of one wavelength downstream of the tower when measured from a wave crest at the tower, and the wake flow behind the tower is strongly unsteady as it is modulated by the waves, while the flow within the tower is relatively simple. For more discussion on the flow behaviour and the interaction with the porous tower, see Santo et al. (2015a).

5. Conclusions

In this paper, blockage due to regular waves with the presence of sheared current is investigated experimentally and numerically. Strongly sheared current profiles were generated experimentally in a wave-current flume using a purposely-built wire structure near the inlet and outlet of the discharge, and a stable sheared profile in space and time could be achieved. The same sheared profiles were reproduced numerically in a numerical wave tank using OpenFOAM, which compare well with the measured profile using a combination of ADV and PIV. The full range of the experimental wave and wave-current conditions was simulated in numerical simulations. However, the numerical simulations were able to be extended to cases with steeper waves which could not otherwise be generated in the present experimental facilities. Two loading scenarios were considered with a space-frame structure model positioned end-on and diagonal to the incident flow. Experiments were conducted using a truss model consisting of mostly vertical and with a few diagonal aluminium cylinders, while a simplified porous tower model as a proxy for the physical truss model was used for the numerical simulations.

Experimental results for the resultant drag on the truss model due to steady sheared current agree well with the numerical simulations as well as the analytical simple current blockage model, for a range of current speeds and two different loading configurations. We observe that under the same input current condition, the end-on loading configuration has higher blockage and hence the drag force is smaller than that of the diagonal loading configuration. The difference in the drag force increases as the current (or loading) increases. The measured drag and the reduced sheared current profile predicted by the SCB model compare relatively well with that of the numerical simulations, suggesting minimum vertical flow interaction within the porous tower. Subsequent numerical flow visualisation confirms there is some downward flow inside the porous tower due to the nature of non-uniform loading of sheared current on a uniformly-distributed resistance of the tower, but the dominant flow interaction is the lateral flow divergence, hence the SCB model based solely on lateral flow divergence is a reasonable approximation in this regard.

For regular waves without current where wave blockage is known to be insignificant, the measured total force between the end-on and diagonal loading configuration is comparable because the truss model is made of predominantly vertical cylinders, and hence the drag area and the inertia volume can be regarded as constant. Using C_d=2.12 and C_m=2.0, the numerical predictions of the peak total forces and shape of the force time history agree reasonably well with the experimental results for smaller wave height. However, the drag force is consistently over-predicted as the wave height increases, presumably due to a Keulagan-Carpenter or a Reynolds number effect. The measured total forces for the end-on and diagonal loading configuration become more different when a significant current is introduced. In general, the diagonal loading configuration yield higher forces compared to the end-on one under the same input condition. This highlights the importance of considering the diagonal case since it is a more critical configuration for loading of the corner piles or other foundation system. Predictions due to the present API recipe using the same C_d and C_m values over-predict the forces for regular waves with inline current, and when C_d is tuned to match the crest of the drag force time history, the predictions from the present API recipe are not able to reproduce the entire measured drag force time history. In contrast, the simulated forces for waves with in-line current (the full blockage recipe) agree well with the experimental results using a single set of consistent C_d and C_m values, both in terms of peak forces as well as complete force time history of drag, inertia and total force. The good agreement demonstrates the validity and robustness of the porous block with an embedded Morison resistance approach in offshore engineering to predict more accurately the actual hydrodynamic forces accounting for the complete wave-current blockage effects.

There is significant similarity in the flow behaviour between regular waves with in-line sheared and uniform current, in that the wake downstream of the tower is strongly modulated by the waves, but the flow within the tower is relatively simple. Overall, the application of a porous block as a simple representation for the complex geometry of real space-frame structures when exposed to combined large regular waves and in-line sheared or uniform current is proven to be a useful approach. An extension of the present model to account for wave irregularity with the presence of current is under development, and will be reported elsewhere.

Acknowledgements

We are grateful for the support from EPSRC (project EP/J010316/1 Supergen MARine TechnologY challenge). We would also like to acknowledge the use of the University of Oxford Advanced Research Computing (ARC) facility in carrying out this work, see http://dx.doi.org/10.5281/zenodo.22558http://dx.doi.org/10.5281/zenodo.22558⟩. The technicians at UCL provided a high quality facility and technical service. The experimental data can be found at http://dx.doi.org/10.5281/zenodo.22558https://www.researchgate.net/project/Data-for-sheared-current-blockage⟩.

Appendix

- Fig. 14 provides a detailed schematic drawing of the truss, together with the loading orientation. The truss can be found at ⟨http://www.terralec.co.uk/chrome_deco_truss__20mm/chrome_deco_truss_1m_straight/28272_p.html⟩, with part number DT-3032.

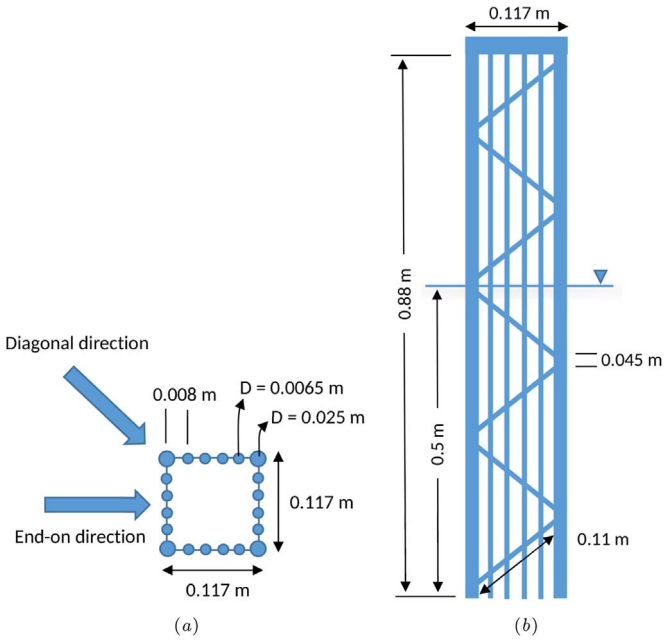

Fig. 14. Schematic diagram of plan (a) and side (b) view of the truss structure (not to scale). The other three vertical sides of the truss follow the same pattern as the one shown in (b).

- Fig. 15 provides the force calibration used in the experiments.
- At lab scale, the measured peak forces are typically ~6 N (c.f. Figs. 10 and 12). Hence, from a depth of 0.5 m scaled to 100 m using Froude scaling (so length ×200, wave period ×14, current velocity ×14), the tower frontal width scales to 23.4 m and the predicted forces become ~47 MN. Forces of this magnitude are consistent with those expected on a typical offshore platform in extreme conditions.

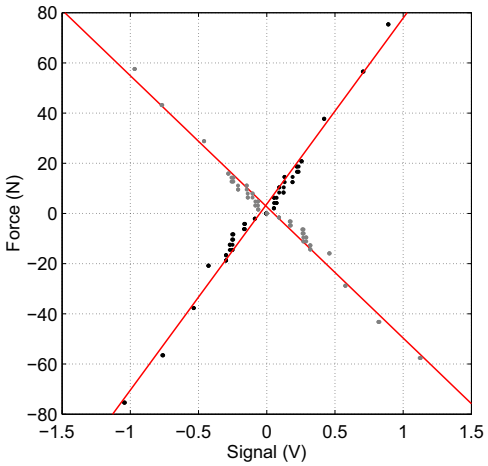

Fig. 15. Plot of measured signal (V) against applied force (N) for the two load cells subjected to compression and tension. The two solid lines are the fitted line used for force calibration.

References

Allender, J., Petrauskas, C., 1987. Measured and predicted wave plus current loading on a laboratory-scale, space frame structure. In: Proceedings of the Offshore Technology Conference, (OTC) 5371.

American Petroleum Institute, 2000. Recommended practice for planning, designing, and constructing fixed offshore platforms–working stress design. API RP2A-WSD 21st Edition with Erratas and Supplements 1, 130–132.

Berberović, E., van Hinsberg, N.P., Jakirlić, S., Roisman, I.V., Tropea, C., 2009. Drop impact onto a liquid layer of finite thickness dynamics of the cavity evolution. Phys. Rev. E – Stat., Nonlinear, and Soft Matter Phys. 79 (3), 036306.

Chakrabarti, S.K., 1996. Shear current and its effect on fixed and floating structures. Adv. Coast. Ocean Eng. 2, 231.

Chen, H., Christensen, E.D., 2016. Investigations on the porous resistance coefficients for fishing net structures. J. Fluids Struct. 65, 76–107.

Draper, S., Nishino, T., Adcock, T.A.A., Taylor, P.H., 2016. Performance of an ideal turbine in an inviscid shear flow. J. Fluid Mech. 796, 86–112.

Fleming, C.F., McIntosh, S.C., Willden, R.H.J., 2013. Tidal turbine performance in sheared flow. In: 10th European Wave and Tidal Energy Conference.

Forristall, G.Z., Cooper, C.K., 1997. Design current profiles using empirical orthogonal function (EOF) and inverse FORM methods. In: Proceedings of the Offshore Technology Conference, (OTC) 8267.

Garrett, C., Cummins, P., 2007. The efficiency of a turbine in a tidal channel. J. Fluid Mech. 588, 243–251.

Gunn, K., Stock-Williams, C., 2013. On validating numerical hydrodynamic models of complex tidal flow. Inter. J. Mar. Energy 3, e82–e97.

Jacobsen, N.G., Fuhrman, D.R., Fredsøe, J., 2012. A wave generation toolbox for the open-source CFD library: OpenFOAM®. Inter. J. Numer. Methods Fluids 70 (9), 1073–1088.

Jensen, B., Jacobsen, N.G., Christensen, E.D., 2014. Investigations on the porous media equations and resistance coefficients for coastal structures. Coast. Eng. 84, 56–72.

Kevlahan, N.K.R., Ghidaglia, J.M., 2001. Computation of turbulent flow past an array of cylinders using a spectral method with Brinkman penalization. Eur. J. Mech.-B/Fluids 20 (3), 333–350.

Kristiansen, T., Faltinsen, O.M., 2012. Modelling of current loads on aquaculture net cages. J. Fluids Struct. 34, 218–235.

Lueck, R.G., Lu, Y., 1997. The logarithmic layer in a tidal channel. Cont. Shelf Res. 17 (14), 1785–1801.

Morison, J., O'Brien, M., Johnson, J., Schaaf, S., 1950. The force exerted by surface waves on piles. J. Pet. Technol. 2 (5), 149–154.

Sanford, T.B., Lien, R.-C., 1999. Turbulent properties in a homogeneous tidal bottom boundary layer. J. Geophys. Res.: Oceans 104 (C1), 1245–1257.

Santo, H., Taylor, P.H., Bai, W., Choo, Y.S., 2014a. Blockage effects in wave and current: 2D planar simulations of combined regular oscillations and steady flow through porous blocks. Ocean Eng. 88, 174–186.

Santo, H., Taylor, P.H., Bai, W., Choo, Y.S., 2015. Current blockage in a numerical wave tank: 3D simulations of regular waves and current through a porous tower. Comput. Fluids 115, 256–269.

Santo, H., Taylor, P.H., Day, A.H., 2015b. Inertia forces on conductor arrays in a jacket model in regular waves. In: Proceedings of the International Workshop on Water Waves and Floating Bodies 2015. IWWWFB.

Santo, H., Taylor, P.H., Williamson, C.H.K., Choo, Y.S., 2014b. Current blockage experiments: force time histories on obstacle arrays in combined steady and oscillatory motion. J. Fluid Mech. 739, 143–178.

Stacey, M.T., Monismith, S.G., Burau, J.R., 1999. Measurements of reynolds stress profiles in unstratified tidal flow. J. Geophys. Res. 104, 10935–10949.

Stagonas, D., Buldakov, E., Simons, R., 2014. Focusing unidirectional wave groups on finite water depth with and without currents. Coast. Eng. Proc. 1 (34), 31.

Stagonas, D., Buldakov, E., Simons, R., 2015. Extreme wave loads on a vertical slender cylinder with and without current. In: The Twenty-fifth International Offshore and Polar Engineering Conference. International Society of Offshore and Polar Engineers.

Stagonas, D., Buldakov, E., Simons, R., 2016. On the focusing of waves on sheared currents in a wave-current flume. Coastal Engineering (under review).

Taylor, P.H., 1991. Current blockage: reduced forces on offshore space-frame structures. In: Proceeding of the Offshore Technology Conference, OTC 6519.

Taylor, P.H., Santo, H., Choo, Y.S., 2013. Current blockage: reduced Morison forces on space frame structures with high hydrodynamic area, and in regular waves and current. Ocean Eng. 57, 11–24.

Zhao, Y.P., Bi, C.W., Dong, G.H., Gui, F.K., Cui, Y., Guan, C.T., Xu, T.J., 2013. Numerical simulation of the flow around fishing plane nets using the porous media model. Ocean Eng. 62, 25–37.